JOURNAL OF THERMOPHYSICS AND HEAT TRANSFER
Vol. 24, No. 1, January–March 2010

Sidewall Effects on Heat Transfer Coefficient in a Narrow Impingement Channel

Mark Ricklick* and J. S. Kapat†
University of Central Florida, Orlando, Florida 32826
and
James Heidmann‡
NASA John H. Glenn Research Center at Lewis Field, Cleveland, Ohio 44135

DOI: 10.2514/1.44166

This paper examines the local and averaged effects of channel height in the presence of sidewalls on heat transfer coefficients, with special attention given to the sidewall behavior. High resolution local heat transfer coefficient distributions on target and sidewall surfaces were computed using temperature sensitive paint, recorded via a scientific-grade charge-coupled device camera, and compared with available literature. This is important, as many of the major correlations related to impingement channels are directly applicable to wide arrays of jets, for which the influence of the presence of sidewalls is minimal. Streamwise pressure distributions were recorded and used to explain heat transfer trends and to determine the thermal effectiveness of each channel. Results are presented for average jet-based Reynolds numbers between 17,000 and 45,000. All experiments were carried out on a large-scale single-row 15-hole impingement channel (with an X/D of 5, a Y/D of 4, and a Z/D of 1, 3 and 5). It was observed that available correlations accurately predict the target surface heat transfer coefficients when the influence of the sidewall is minimal, typically at larger channel heights and lower Reynolds numbers. Smaller channel heights tend to outperform larger channels, when considering thermal effectiveness and channel-averaged heat transfer rates, due to the increased heat transfer on the channel sidewalls.

Nomenclature

A	=	cross-sectional area, m
atm	=	atmospheric
C_d	=	discharge coefficient
c	=	crossflow value
ch	=	channel value
D	=	jet diameter, m
D_{ch}	=	channel hydraulic diameter, m
eff	=	effective value
f	=	friction factor
G	=	mass flux, kg/m^2s
h	=	heat transfer coefficient, W/m^2K
htr	=	heater surface
j	=	jet value
L	=	test section length, m
loss	=	quantity lost to the environment
P	=	static pressure, Pa
pl	=	plenum value
q''	=	heat flux, W/m^2
R	=	gas constant for air, $J/kg \cdot K$
Re	=	Reynolds number
r	=	heater resistance
T	=	static temperature, K
U	=	velocity of flow within the channel, m/s
V	=	voltage, V
w	=	wall value
X	=	streamwise coordinate, m
Y	=	spanwise coordinate, m
Z	=	vertical coordinate, m
γ	=	ratio of specific heats for air
η	=	thermal effectiveness
ρ	=	density of air, kg/m^3
0	=	baseline (pure channel) value

Presented as Paper 1430 at the 47th AIAA Aerospace Sciences Meeting including The New Horizons Forum and Aerospace Exposition, Orlando, FL, 5–8 January 2009; received 1 April 2009; revision received 19 August 2009; accepted for publication 30 August 2009.

*Graduate Research Assistant, Laboratory for Turbine Heat Transfer and Aerodynamics, Department of Mechanical, Materials, and Aerospace Engineering, 813 Murdock Boulevard. Student Member AIAA.

†Professor, Laboratory for Turbine Heat Transfer and Aerodynamics, Department of Mechanical, Materials, and Aerospace Engineering, 4000 Central Florida Boulevard. Member AIAA.

‡Turbomachinery and Heat Transfer Branch, 21000 Brookpark Road, Mail Stop 5–11.

I. Introduction

HIGH-PERFORMANCE turbine airfoils, in both propulsion and power generation systems, are typically cooled with a combination of internal cooling and impingement channels. Numerous cooling techniques are used in a variety of locations, depending on the application and the required heat removal rate. In some applications, such as airfoil leading edge cooling or the cooling of various endwall locations, impingement channel cooling has become the preferred method. In such applications, the jets impinge against a target surface and then exit along the channel formed by the jet plate, the target plate, and the sidewalls, then exiting near the airfoil edge (typically being used for film cooling). Local heat transfer coefficients (HTCs) are the result of both the jet impact as well as the channel flow produced from the exhausted jets. Numerous studies have explored the effects of jet array and channel configurations on both target and jet plate HTCs. However, little work has given attention to the sidewalls, which could potentially contribute a considerable amount of heat transfer, especially when the channels become narrow. As designers strive to design engines that operate at higher temperatures and efficiencies, it will become necessary to develop a better understanding of the complex flow and heat transfer processes that go on inside the engines and the complex cooling channels within them.

The motivation behind impingement channel cooling is to remove the heat at a location close to its source, so that the heat removal process is thermodynamically more efficient, while attempting to maintain the relatively uniform heat transfer characteristics of pure channel cooling. Because heat comes from the hot gas path in an

airfoil, the impingement channel cooling technique places the cooling ducts beneath the airfoil hot surface. Because of the limitation of available space, the cooling ducts are small in a cross-sectional area. The air used to cool the various parts inside the turbine is often bled from the compressor, therefore reducing the maximum attainable efficiencies. It is therefore extremely important to effectively cool the turbine with a minimal amount of coolant. At the same time, it is desired to maintain nearly uniform temperatures on the component surfaces in order to minimize thermal stresses. For this reason, impingement arrays and channel designs must be optimized for efficient heat removal. In some instances, it may be necessary to incorporate sidewalls into the design, such as for the support of an impingement insert within a hollow blade. The presence of this sidewall may potentially aid in the heat removal process, acting to draw the heat away from the hot target surface. A second stagnation region would also exist where the wall jet formed during impingement collided with the sidewall. This second impingement would be beneficial, increasing the heat transfer in this area. The HTC cannot be assumed to be circumferentially uniform in these small cooling ducts due to the complex flow structure involved; thus, any predictive tools that may be used to evaluate such cooling techniques must be validated in a similar situation.

The purpose of this paper is to understand the effects of the varying channel height on two wetted surfaces, with special attention to the sidewalls, in a narrow impingement channel. These results will then be compared with existing impingement channel correlations for large arrays in an attempt to assess their validity in the presence of sidewalls. This is important, as it will be shown that the sidewalls can contribute significantly to the overall heat transfer effects of a narrow channel, and the prediction capabilities of the available correlations must be validated. This is accomplished in a simple flow arrangement: namely, a set of impingement holes in a narrow channel.

Over the years, numerous experiments have been performed by various groups to investigate the flow physics of impingement channel cooling techniques. Some of the original works in this area presented various averaged results of the target wall Nusselt number, as well as various flow characteristics. As measurement techniques have improved, researchers have begun to contribute local results. Effects of jet array configurations, geometric parameters (channel dimensions and hole spacing), as well as crossflow on the target wall Nusselt number have been adequately reported. These investigations have allowed designers to more effectively implement impingement channel cooling in a variety of applications, including internal cooling configurations in turbine airfoils (such as that described by Taylor [1]). In this application, as seen in Fig. 1, an insert is placed within the hollowed core of the airfoil. Air is then forced from the central portion (which acts as a plenum) through the small impingement holes, where it then impinges against the backside of the hot surface of the airfoil.

Early investigations by Florscheutz et al. [2–4] presented array-averaged, as well as spanwise-averaged, Nusselt numbers with resolutions of one-third to two times the streamwise hole spacing. A one-dimensional momentum flux model was also developed to predict channel flow distributions, which agreed favorably with the experimental results. Effects on the Nusselt number due to array configurations (inline versus staggered), channel dimensions, as well as the amount of crossflow, were reported. Correlations were developed based on local jet Reynolds numbers, the Prandtl number, the crossflow to jet velocity ratio (G_c/G_j), the geometric parameters of hole spacing (X/D and Y/D), and the channel height (Z/D); all were normalized by the jet hole diameter. Tests were performed for jet Reynolds numbers between 2500 to 70,000, for G_c/G_j from 0 to 0.8, for X/D between 5 and 15 for the inline pattern, for Y/D between 4 and 8, and for Z/D between 1 and 3. Their work showed that flow distributions were only dependant on the discharge coefficient, number of impingement rows, and the product of the geometric parameters Y/D and Z/D. Their results also showed that the most uniform Nusselt number distributions resulted when, as expected, the flow distributions were most uniform. This occurred at higher values of $(Y/D)\cdot(Z/D)$. For these cases, the local jet Reynolds numbers did not vary significantly in the streamwise direction and resulted in lower exiting G_c/G_j values. The most highly nonuniform results were seen when the exiting values of G_c/G_j were the highest ($\sim$0.75). It was also seen that the trend in Nusselt numbers versus G_c/G_j shifts from a monotonic decreasing trend to one that shows a minimum as X/D and Y/D increase, and Z/D decreases. Therefore, there were cases for which the Nusselt number began to increase in the streamwise direction. This behavior was explained by the fact that the crossflow for these cases provided a significant contribution to the heat transfer without significantly degrading the downstream jets. Crossflow effects versus Z/D increased as the aspect ratio X/Y increased. These results show the complexity of the flowfield generated in this cooling application and are the major reason for the complex correlation developed.

As Florshuetz et al. [2] obtained this data in a spanwise-averaged fashion, using a segmented isothermal target plate, the spanwise variations were not captured. It was discussed, however, that these effects are important, as the crossflow produced by the exhausted jets

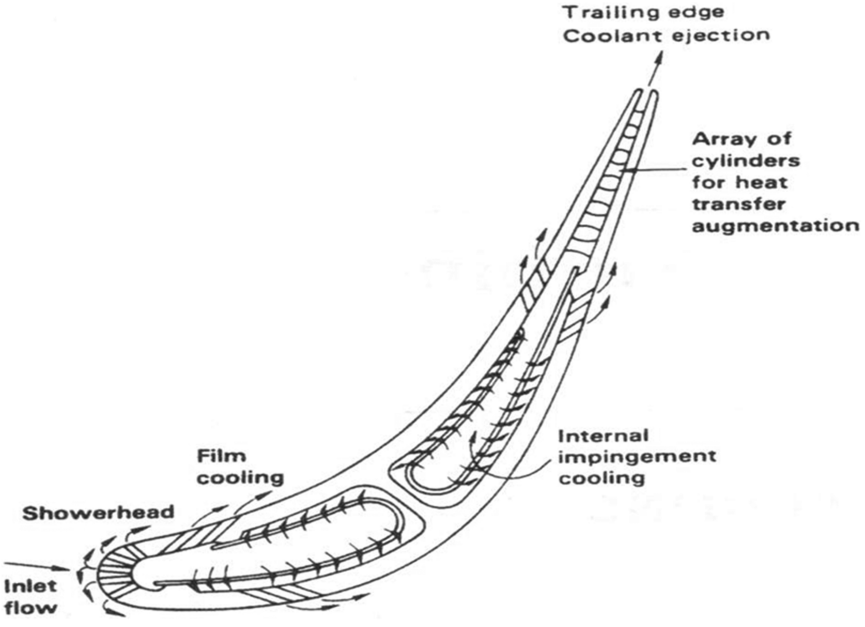

Fig. 1 Impingement channel application.

is not uniform and may become channelized, allowing downstream jets to continue to impinge the target surface. The correlation developed in this work is of the form

$$Nu = A(Re_j)^m \left\{1 - B\left[\left(\frac{Z}{D}\right)\left(\frac{G_c}{G_j}\right)\right]^n\right\} Pr^{1/3}$$

where the constants A, B, m, and n are dependent on the channel geometry and array pattern.

Al-Aqal [5] conducted experiments to determine heat transfer distributions on two of the walls (target and jet plates) of a narrow channel with jet impingement and crossflow. The experiments had three different configurations of impinging jets, with variations in the number of holes, while maintaining equal total hole areas. These geometries were tested for a range of jet Reynolds numbers between 14,000 and 33,000. The results of the target wall Nusselt number versus the axial distance were presented and showed an oscillating trend that diminished with X/D, with peaks at the impingement locations. The optimal distance for jet-to-target plate spacing was found to be $Z/D_j = 2.67$ for both the jet-issuing and target plates for the six-hole case. The 24-hole case optimum spacing was $Z/D_j = 2.67$ for the target plate and $Z/D_j = 5.33$ for the jet-issuing plate. The 54-hole case values were $Z/D_j = 8$ for both the jet-issuing and target plates. Local heat transfer on the target plate showed much more uniformity at small jet-to-target spacing than large jet-to-target spacing.

Numerous other works have explored different aspects of impingement channel cooling and its ability to remove heat from various components in the turbine system. Lucas et al. [6] conducted several local heat transfer studies of an enclosed impinging jet, investigating the effects of the thermal boundary conditions at the jet plate. Their work showed that jet plate temperatures tend to have some effect on the target surface, due to a recirculation zone formed between the jet and the jet plate. Van Treuren et al. [7] continued this investigation and its application to rows of jets impinging in a turbine representative channel. The coupling between the upper and lower surfaces was further explained, and contour results were presented that highlighted the effects of the crossflow in the downstream directions. There was an increasing effect of crossflow in the downstream direction, where the heat transfer away from the stagnation region remained high. A detailed analysis of an engine representative impingement channel cooling system was also studied by Son et al. [8]. Others, such as Annerfeld et al. [9] and Mushatat [10], investigated the effects of surface features within these channels.

The available literature suggests that heat transfer distributions within impingement channels are dependent on numerous factors, such as hole-to-hole spacing, channel cross-sectional dimensions, as well as jet and crossflow mass flow distributions. The current study intends to investigate the effects of channel height and coolant flow rate on the pressure and heat transfer distributions. Although the previous literature provides accurate data for jet impingement channels with crossflow effects, there has not been significant focus on the additional effect that comes from the presence of sidewalls nor the heat transfer rates on these surfaces. The present study focuses on impingement channels with a strong influence from the sidewalls, on a relatively narrow channel. Local measurements on all wetted surfaces will be taken using temperature sensitive paint (TSP), which has the capability of producing high-resolution images (on the order of 10–15 pixels per millimeter). These features will be investigated in the current study for average jet-based Reynolds numbers of 17,000 and 45,000. All experiments were carried out on a large-scale single-row 15-hole impingement channel, with an X/D of 5, a Y/D of 4, and a Z/D of 1, 3 and 5.

II. Experimental Setup and Data Reduction

The experimental setup is designed to resemble a narrow impingement channel in a turbine airfoil. The test channel includes a multiple jet-issue plate and a target plate enclosed by walls on either side. The first jet hole is located at an X/D of 5. At X/D equal to zero, the channel is closed so that the exhausted jet flow is restricted to flow in the downstream direction (of increasing X/D). The channel then simply exits into the atmosphere. The walls are designed so that the test section can be easily modified to change both channel width and channel height. The test section is constructed from 25-mm-thick acrylic. Jet holes were counterbored to maintain a jet length of 1 diameter. The use of a jet with a small length-to-diameter ratio is common in the literature ([2,3,6], for example) and results in a relatively flat jet velocity profile. Although some other authors have explored the effects of hydrodynamically developed impinging jets, the undeveloped profile is more applicable to turbine airfoil applications. The counterbore diameters were three times that of the jet hole. Flow from a vortex blower is fed to the jet plate via a plenum outfitted with flow straighteners and screens. Inlet air temperatures are maintained using an air-to-water heat exchanger, and the flow rates are controlled through the adjustment of control valves. The plenum design, constructed from two side plenums that feed a central plenum, allowed data to be captured from the jet plate, although it was not included in the current study. Flow conditioners were placed in the side plenums, with the central plenum allowing optical access of the jet plate. The opening area between the two plenums was over 30 times that of the total area of the jets, creating negligible velocities within the plenum and plenum inlet. Additional side and target walls were constructed and outfitted with rows of pressure taps, located between each jet hole. These taps allowed for pressure profile measurements for determining flow distributions within the channel. The test section has an X/D of 5, a Y/D of 4, and a variable Z/D of 1, 3, and 5. The impingement channel configuration and setup is shown in Fig. 2.

TSP provides a non intrusive method for measuring the temperature of a surface. The paint is polymer based and includes luminescent molecules that, when excited by a light of a certain wavelength, emit light of a longer wavelength. As a result of thermal quenching, the intensity of light emitted by the luminescent molecules decreases as the temperature increases. Once the paint is calibrated, temperatures can be determined from intensity values that are read by a single charge-coupled device (CCD) camera. TSP is a reliable method for determining temperature, as it is accurate within 0.8°C [11]. Using TSP, high-resolution local HTC distributions on all four wetted surfaces will be recorded via a scientific grade CCD camera.

TSP temperatures were confirmed by three T-type thermocouples, placed at various locations along each channel wall, with acceptable

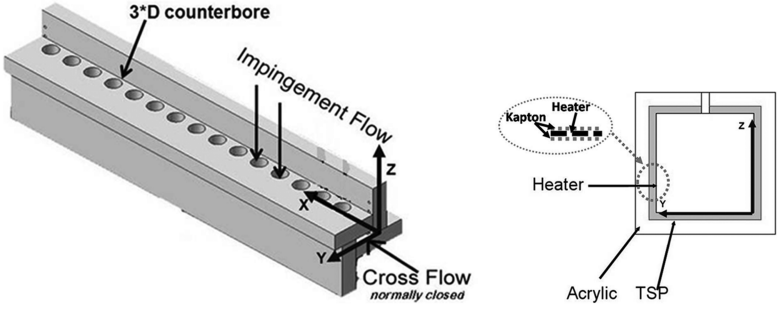

Fig. 2 Impingement channel configuration.

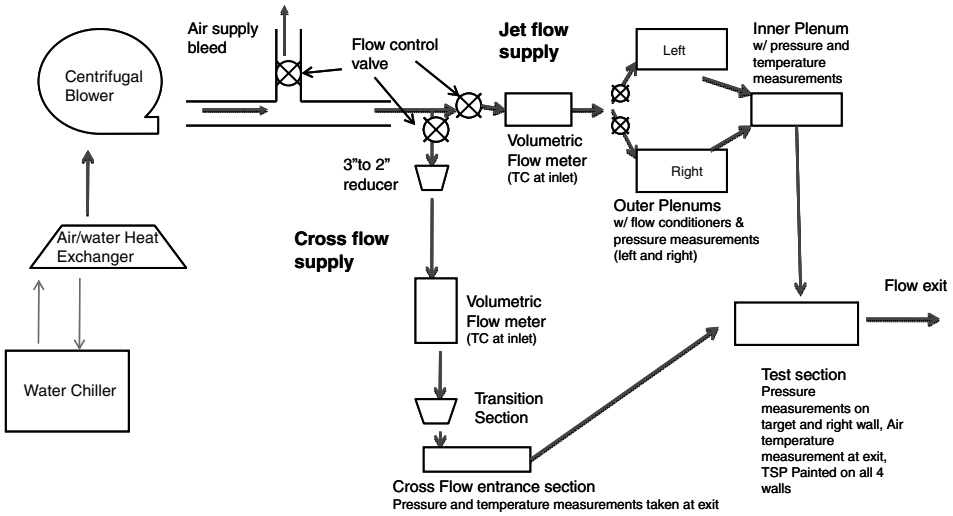

Fig. 3 Flow loop.

agreement within experimental uncertainty. Plenum and ambient temperatures were also recorded with similar thermocouples, all recorded with a Measurement Computing data acquisition system connected to a standard PC. Maximum uncertainties from thermocouple readings were $\pm 1°C$. Minimum wall-to-plenum temperature differences were maintained well above 20°C in order to minimize uncertainties.

Figure 3 shows the impingement channel flow loop. A single vortex blower is used to supply impingement flow. Air that is to be impinged goes through flow conditioners located in the right and left plenums. The separated plenum design allows for images to be taken of the jet plate from above. The current test matrix is given in Table 1.

The plate discharge coefficient was found by sending air through the jet plate without the surrounding walls, allowing it to exhaust into the atmosphere (as is typically done in the literature). The plenum and atmospheric pressures were measured using a Scanivalve pressure scanner and recorded with another Measurement Computing data acquisition system ($\pm 0.05\%$ uncertainty), and the mass flow rate was measured using a Venturi flowmeter ($\pm 1\%$). The calculated C_D values do not vary significantly over the pressure ratios tested and are therefore assumed constant. A similar trend was observed in the literature [2]. The presence of the walls and the target, as well as the sidewalls, leads to concern of potential effects on the discharge coefficient. The added effects of crossflow only increase this concern. However, the work performed by Florschuetz and Isoda [3] suggests that crossflow and channel height effects will have no effect on the discharge coefficient when the channel height is larger than 1 diameter, and the crossflow-to-jet mass flow ratio does not exceed some critical value. Beyond this critical value, at small channel heights, the discharge coefficient tends to decrease slowly until the mass flux ratio exceeds unity. Beyond this point, the discharge coefficient cannot be assumed to be unaffected by the crossflow. Minimal effects from this were only seen for case 1 of this study and have thus been neglected. Regarding the sidewall presence, consistency between calculated mass flow rates and those measured by the flowmeter confirmed our choice of discharge coefficient.

Once the array average discharge coefficient was determined, the channel was assembled, with the two walls instrumented with pressure taps. Pressure profiling tests were taken under a no-heat condition, so that the fluid properties could be assumed constant. Static channel, plenum, and atmospheric pressures were recorded (again with the Scanivalve). The side and target surface pressure profiles were compared for consistency, as it was seen in [2] that these pressures should be equal. Pressure profiles did not vary more than 12 Pa from wall to wall. These data allowed calculation of the pressure ratio distribution and resulting mass flow distributions.

The ratio of the jet mass flux and average jet mass flux, $G_j/G_{j\text{avg}}$, was calculated using the obtained C_D values and the one-dimensional model developed in [2]. This model was then compared with the calculated $G_j/G_{j\text{avg}}$, based on measurements made in the pressure profiling test and the C_D test using Eq. (1), which accounts for compressibility effects. This was necessary due to the large variations in pressure between the channel and the plenum, although maximum jet Mach numbers did not exceed 0.29:

$$G_{j_i} = C_d \cdot P_{\text{pl}} \left(\frac{P_i}{P_{\text{pl}}}\right)^{[(\gamma+1)/(2\gamma)]} \times \sqrt{\left\{\frac{2\gamma}{\gamma-1}\frac{1}{R\cdot T_{\text{pl}}}\left[\left(\frac{P_{\text{pl}}}{P_i}\right)^{[(\gamma-1)/\gamma]} - 1\right]\right\}} \tag{1}$$

The pressure ratio was that between the plenum and the measured value at the jet hole, which was interpolated between the recorded static pressure values. The assumption that the pressures at the jet can be interpolated along the channel is validated again by the work done in [4]. Here, a pressure probe was traversed along the channel, resulting in smooth pressure profiles along the length of the channel. All air properties were taken at the plenum conditions in the current work.

Next, an estimated ratio of crossflow mass flux to jet mass flux (G_c/G_j) was found using another equation, developed in the model in [2], and then compared with experimentally calculated values. Crossflow mass fluxes (G_c) were calculated from the collected experimental data, knowing that the mass flow exhausted from the preceding jets is equal to the mass flow through the channel up to the current jet. It is calculated using the following formula:

$$G_{c_i} = G_{j_i}\left(\frac{A_j}{A_c}\right) + G_{c_{i-1}} \tag{2}$$

$G_j/G_{j\text{avg}}$ and G_c/G_j values determined experimentally were plotted against the models developed by Florschuetz, shown in Figs. 4 and 5.

With knowledge of the channel pressure and flow distribution, it is also possible to calculate a representative channel friction factor, so that it may be compared with that of a smooth pipe. Comparisons between different configurations can then be made, allowing some insight to the amount of extra work that has to be done to obtain the high HTCs. This value should be representative of the frictional work

Table 1 Test Matrix

Test	*Re*	*X*/*D*	*Y*/*D*	*Z*/*D*
Case 1	17,500	5	4	1
Case 2A	17,900	5	4	3
Case 2B	45,000	5	4	3
Case 3	43,000	5	4	5

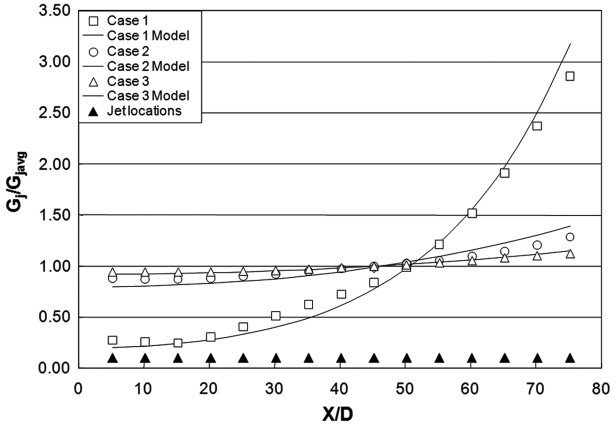

Fig. 4 Jet mass flux distribution.

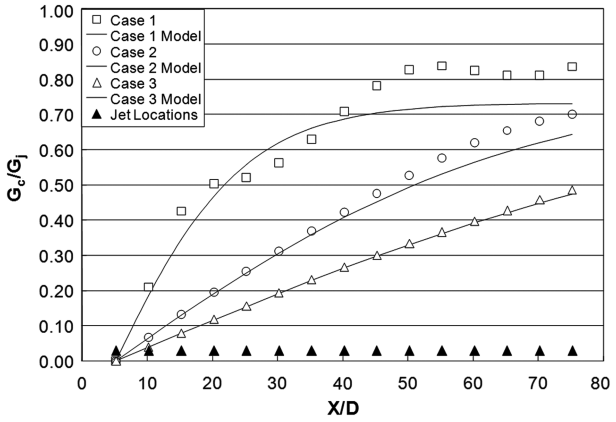

Fig. 5 Crossflow-to-jet mass flux ratio.

required to push the fluid through the impingement array and channel. The channel friction factors are calculated according to

$$f = \frac{(P_{\text{pl}} - P_{\text{atm}})}{L} \frac{D_{\text{ch}}}{2\rho U^2} \tag{3}$$

The pressure drop includes the drop through the array plus the work required to push the flow out of the channel. The plenum density and the maximum channel velocity were used for these calculations. For comparison, the Blasius solution for the friction factor through a smooth pipe is used. This friction factor is defined according to Eq. (4), for which the maximum channel Reynolds number was used in the correlation:

$$f_0 = 0.184 \cdot Re^{-1/5} \tag{4}$$

Before testing, ambient heat losses were quantified by insulating the interior of the channel and applying even heating to the test section walls. After several steady-state temperatures were reached, the amount of heat lost to the environment was then correlated against the temperature difference between the wall and the environment. For each case tested, temperature distributions on each wall are recorded using TSP, as mentioned. Heat fluxes on the target wall and two sidewalls are calculated from the applied voltages and measured heater resistances. The heaters were custom-manufactured foil heaters that were used to generate a heat flux on each wall. The heaters were constructed from single strips, each one-hole-diameter wide, so that as the channel dimensions were varied, individual heaters could be turned on or off as needed (as shown in Fig. 6). The heaters were enclosed in 0.5-mm-thick Kapton tape; this aided in attaching the heaters to the wall as well as maintaining minimal lateral conduction effects. The potential temperature drop between the flow surface and the TSP was accounted for during HTC calculations, typically on the order of 1°C. The effective flux, typically on the order of 6000–8000 $\text{W}/\text{m}^2\text{K}$, is then the difference between the applied flux and that lost through the test section:

$$q''_{\text{eff}} = \frac{(V^2/R) - q_{\text{loss}}}{A_{\text{htr}}} \tag{5}$$

Reference temperatures used in the HTC calculations are taken to be the plenum temperature, as is typically done in impingement and impingement channel applications. Using the jet temperature is assumed to be valid for these scenarios, because the high velocity jet has little time to pick up heat before it impinges against the target surface. However, as discussed in [12], this assumption is quite accurate even when compared with calculations that consider the potential increase in bulk temperature. The HTC is then defined according to

$$h = \frac{q''_{\text{eff}}}{T_w - T_{\text{pl}}} \tag{6}$$

This equation is solved for every pixel in the acquired TSP image. The result is a local distribution of HTC values on the wall. Results were then averaged in the spanwise direction, yielding HTC versus streamwise distance (X/D). Target wall streamwise averages were also taken for each jet location, so that our results could be easily compared with correlations found in the literature, which predicted average HTC at a resolution of every jet location. These values were computed by averaging the spanwise-averaged results a half a pitch before and after each jet location. Finally, recorded HTC results are compared against the correlations developed in [2], as well as the predictions for smooth channel HTC, using the well known Dittus–Boelter correlation. A Reynolds number, based off of the channel hydraulic diameter and the mass flow rate (up to a point) are used in this correlation, with properties defined at the film temperature. This comparison will aid in the analysis of the effects of the channel sidewalls and the extent of the benefits due to impingement. Although the Dittus–Boelter correlation is valid only for fully developed flow, with the HTC defined using a local bulk temperature, the comparison gives an idea of the enhancement due to the effects of impingement in that location. It is expected that there would be some effect due to the use of a jet-to-wall temperature difference. However, as shown in [12], these differences in reference temperature produce minimal changes in HTC, around 20% near the exit of the channel. This comparison becomes most appropriate near the end of the channel where the crossflow effects have become dominant.

An area-averaged HTC is then compared with a channel-averaged Dittus–Boelter estimate. To compare the effectiveness of the different cooling scenarios, a thermal effectiveness was defined, assuming constant pumping power between the cases according to

$$\eta = \frac{h/h_0}{(f/f_0)^{1/3}} \tag{7}$$

Area-averaged HTCs were used, as well as maximum baseline values (calculated at the channel exit), for this comparison. Although other methods of comparison are possible, the present method allows for a fair comparison of the channel configurations against a smooth pipe of equal total mass flow rate.

Uncertainties were determined using the Kline–McClintock second power relationship. Effects of instrumentation, data acquisition, and calibration techniques, as well as environmental variations, were all accounted for in the analysis. The major relevant components of uncertainty are the Reynolds number of 8.50%, the h of 12.30%, and the f of 8.73%. The worst case results are presented with a 95% confidence level.

III. Flow Distribution

The discharge coefficient was measured as discussed previously, resulting in an average value of 0.86 (±0.7%), typical of jet holes of this shape. The flow distribution results presented here were first

reported in [12] and help validate our test setup, as well as explain the various trends in HTC that are observed.

The comparison of the recorded jet mass flux to that predicted in [2] is presented in Fig. 4. It can be seen that cases 2 and 3 are nearly linear and very similar in their $G_j/G_{j\text{avg}}$ values. These cases fall closely to the model developed in [2] (as plotted in Fig. 4), suggesting that there is little interaction between the jets in the spanwise direction (as only one row was tested in the current study) and that basic fluid mechanics (described by the control volume analysis in [4]) drive the flow distributions within these flow regimes. Case 1, as mentioned earlier, has the smallest Z/D value, and thus has the greatest acceleration of crossflow (which can be seen in the plot). The curve follows a more exponential trend. Florschuetz et al. [2] also note this trend for their smallest Z/D case (also equal to 1), which exhibits a similar behavior.

Crossflow mass flux distributions are presented in Fig. 5 and compared with [2]. Results are normalized by the local jet mass flux. It can be seen that cases 2 and 3 follow a nearly linear trend that increases with X/D, which follows the $G_j/G_{j\text{avg}}$ data and is also nearly linear. It would be expected that these cases would yield the most uniform HTC in the streamwise direction, according to [2]. Case 1 has a nonlinear trend. At low X/D values, G_c/G_j increases sharply until an X/D of 35, where it flattens out at $\sim$0.85. The experimental data do not follow the model as well as in the other three cases. Similar results were observed in Florschuetz's data for cases with Z/D of 1. This discrepancy was later explained by [3] to be a result of the channel height and the effect of a highly accelerating crossflow on the jet discharge coefficient. It was explained that as the value of G_c/G_j exceeds some critical value (on the order of 0.75–1) the discharge coefficient begins to decrease. These effects become more significant as this ratio is pushed further beyond this critical value, which is dependent on the channel configuration. The effects are assumed to be small in this case, because the calculated and measured mass flow rates matched relatively well for case 1, and only an overall trend is needed to explain our results.

Because of the development of crossflow, the channel pressure decreases with an increase in velocity within the channel. This negative pressure gradient is required to push the exhausted jet flow out of the channel. As the plenum pressure is held constant, a variation in pressure ratios then exists, which results in a variation in the jet and channel Reynolds number in the downstream direction. The jet mass flow distribution and crossflow development balance each other within the channel. This characteristic is captured in the previous figures, but it can also be represented in the form of Reynolds number distribution along the channel for both the jet and the channel (shown in Fig. 7). The channel and jet Reynolds numbers are defined by their respective diameters, and the channel Reynolds number is that which exists up to the particular jet. This plot will aid in explaining the thermal effectiveness of each channel, as the Reynolds number is used for baseline comparisons.

As discussed earlier, a friction factor was computed for each channel and, compared with the smooth channel estimate, calculated at the highest channel Reynolds number. Because the manner in which these friction factors were calculated, they mainly serve as a comparison between different configurations, not between different cooling methods. Nevertheless, the results should give some insight into losses associated with each channel configuration. The normalized friction factor is plotted in Fig. 8. We can see from this plot that, as the cases progress, the friction augmentation is increased. Several factors contribute to this, including the definition itself. It is interesting to note that although case 1 shows a friction factor that is less

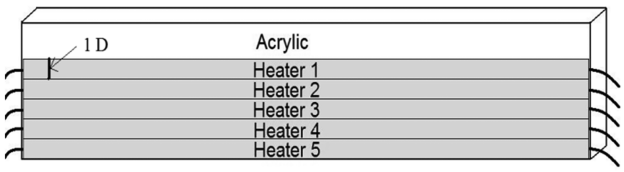

Fig. 6 Heater configuration.

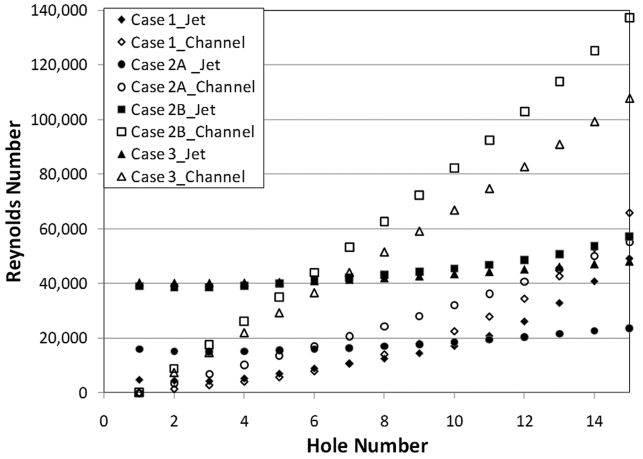

Fig. 7 Reynolds number distribution.

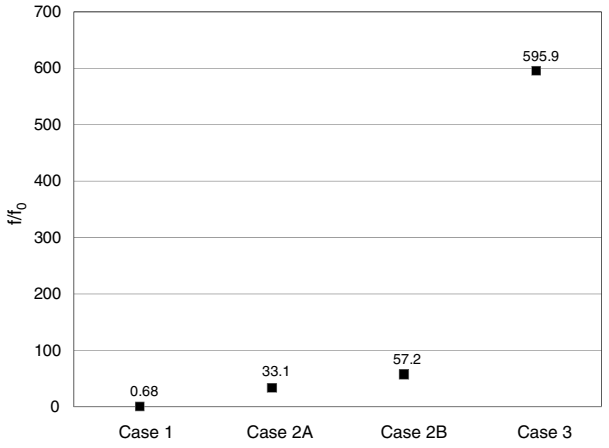

Fig. 8 Normalized friction factor.

than the smooth channel prediction, the largest pressure ratios were required to achieve this flow rate. This is a direct result of the flow distribution within the channel. The crossflow develops most rapidly, with some of the largest velocities overall, near the channels exit. As the calculated friction factor is normalized by the predicted value at this location of maximum velocity, the augmentation is less than unity. However, with the remaining cases, the crossflow distribution is much more uniform (as shown previously), resulting is less drastic variations in velocity. The crossflow within the channel for case 3, for example, increases linearly, so that the pressure drop along the channel consistently increases. However, as the channel height is reduced, the variation along the channel becomes greater, affecting the calculated friction factor along the channel. The effects of this distribution will become most apparent when considering the thermal effectiveness of the channel.

IV. Heat Transfer Results

A. Validation

Heat transfer data are presented as both local surface HTC plots, with an average resolution of 15 pixels per millimeter, and as spanwise-averaged results, with an average resolution of 2 pixels per millimeter. The spanwise-averaged data resolution is decreased to reduce the effects of noise in the data. Tests were conducted on a constant heat flux surface, with wall temperatures recorded via TSP measurements, inlet air temperature measured with a thermocouple, and air temperature change measured with a thermopile rake. The white stripes across the data are double-sided tape where the heater was attached to the acrylic surface. Heat transfer measurement techniques were validated by setting up a pure channel flow scenario by plugging the jet holes and introducing only crossflow into the

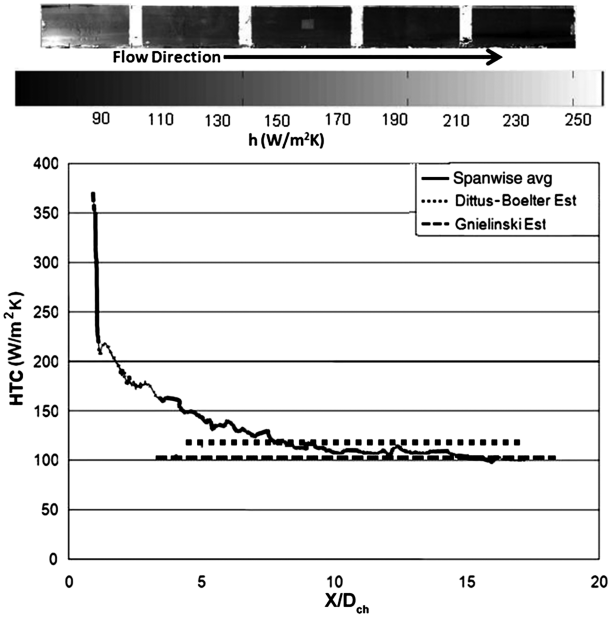

Fig. 9 Validation results.

impingement channel. An entrance section of 30 hydraulic diameters was used to allow the flow to become hydrodynamically fully developed before entering the heat transfer test section. The flow rates were measured with a low-loss Venturi flowmeter. The calculated heat transfer results were compared against accepted pipe flow correlations (Gnielinski and Dittus–Boelter [13]). Fluid bulk temperature for the validation case was assumed to increase linearly across the test section from the inlet-to-exit air temperatures, as is typical for isoflux channel flow conditions. Surface and spanwise-averaged plots of the resulting sidewall HTCs for the validation test are seen in Fig. 9. Similar results were observed on the remaining surfaces.

From Fig. 9, it is evident that the recorded values behave as expected for a pure channel flow case. As expected, there is a high initial HTC at the inlet (due to thermal boundary layer development) followed by a smooth decay as the flow becomes thermally fully developed. At 10 hydraulic diameters, the HTC becomes nearly constant, as is expected for turbulent pipe flow. From the spanwise-averaged plots, it can be seen that our data fall nicely within the uncertainty bands of the two accepted correlations.

B. Impingement Results

Heat transfer results are compared based on variations in the channel height and the average jet Reynolds number. As discussed earlier, there are numerous other parameters also affecting the heat transfer in these channels. As these parameters are changed, flow structures within the channel are expected to be altered as well (as discussed in the literature). Two of the major contributors to heat transfer in these channels, however, are the successful jet impingement and the crossflow that results. The same domain is captured in both the local and averaged results.

Target wall heat transfer profiles are shown in Fig. 10. From this local data, the effect of the accumulation of crossflow can be seen (which has been discussed to some extent in previous literature). The distinct stagnation point becomes less evident, whereas the overall spanwise HTC becomes more uniform as one moves downstream for all cases. The majority of the existing literature has studied channels with fewer impingement holes, on the order of 8–10. However, for the current scenario, 15 jet holes are used, yielding appreciable crossflow effects. We see from this data, that for cases 1, 2A, and 2B, the crossflow velocity was great enough to produce substantial heat transfer rates (even without the direct influence of the jets) for all Reynolds numbers. However case 3 results show a flat profile once the crossflow effects have dominated the impingement effects. This flatter profile is most likely due to the tall channel size, which would

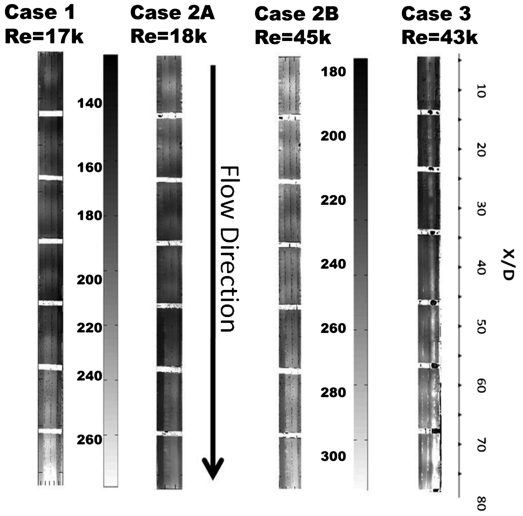

Fig. 10 Target surface heat transfer results.

produce slower crossflow velocities not quite high enough to remove large amounts of heat. Also, as discussed in [6], as the channel height is increased, a recirculation zone near the jet plate and jet becomes substantial, tending to increase the temperature of the jet before impact. This would slightly decrease the heat transfer rate due to the jets. This trend decreases with decreases in the channel height. Also evident from the G_c/G_j plots is the buildup of crossflow is less significant for case 3. Case 3 tended to produce the poorest jet performance, as the large Z/D prevented proper impingement, especially in the presence of crossflow. This is evident when comparing to case 2B, in which stagnation points are seen for several X/D downstream; whereas with case 3, they are not as distinct. An unusual effect was seen for case 1, in which the crossflow actually produced HTC values higher than the upstream impingement values, where the jets have not yet been deflected. This increase in heat transfer is due to the significant amount of crossflow near the exit of this channel. This small channel height and large crossflow acceleration also resulted in a larger channel pressure drop.

From Fig. 11, we see the local HTCs for the sidewalls. We see, initially, the sidewall suffers from very nonuniform heat transfer. The lower portion of the wall tends to have the highest HTC (primarily a result of the second stagnation region) formed from the resulting wall jets. These results seem to be largely affected by the Z/D. For example, with case 1, it is initially very evident where the wall jet is interacting with the sidewall. Only after significant crossflow has developed does the profile become uniform. For the larger Z/D cases near the first few jets, the bottom portion of the right wall has comparable values with the exiting portion. As the crossflow develops,

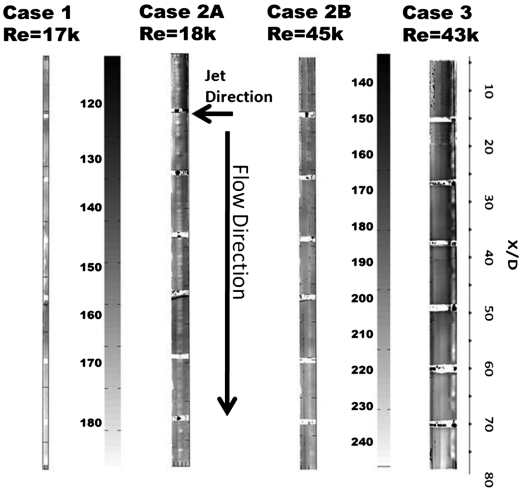

Fig. 11 Sidewall heat transfer results.

this peak diminishes (most likely due to the interactions between the crossflow and the wall jets), which would eventually prevent the wall jets from impinging against the sidewalls. However, the increase in crossflow leads to an increased heat transfer in the downstream direction. Cases 2A and 3 seem most similar, although cases 1 and 2A also exhibit similar behaviors. This similarity suggests that there is an optimal jet Reynolds number and Z/D combination that would provide uniform heat transfer results on the sidewalls.

The effect of the crossflow developing also leads to the HTC increasing almost linearly after $X/D = 40$ for all cases except case 2B. Before this point, however, the HTC is almost constant for all cases. Only case 1 has obvious peaks resulting from the impacting jets. For both comparisons, the smaller channel size produces higher HTCs (as is expected), due mainly to the increased crossflow velocities. Interesting to note, however, is the fact that case 2B yields almost entirely constant values across the entire length. This nearly constant profile could be ideal for designers seeking to produce uniform sidewall temperatures. Also worth noting is the rate of increase in HTC for case 1 after $X/D = 50$. This increase must be the result of the rapid rise in crossflow velocities for this case, which directly leads to increased HTCs.

C. Comparison to Literature

To examine the validity of the existing correlations in the presence of sidewalls [1], spanwise-averaged results are compared against predicted values for both a smooth channel as well as an impingement channel. Both the target surface, as well as the sidewall spanwise-averaged plots, are presented along with per jet averages for the target surface. Uncertainty bands are based on worst case values reported in the appropriate literature: $\pm 12.3\%$ for presented the HTC results, $\pm 18\%$ for the Florschuetz correlation, and $\pm 20\%$ for the Dittus–Boelter correlation. Comparisons are made against smooth channel predictions, as discussed earlier, using the channel Reynolds number distribution shown previously. As mentioned, this will aid in distinguishing how beneficial the flow arrangement is, compared with a standard smooth pipe cooling arrangement, when run at the same channel Reynolds number.

For case 1, with a $Z/D = 1$, the side and target surfaces perform similarly up to an X/D of 45. These results are shown in Fig. 12. At this point, the target surface continues to increase in HTC, whereas the sidewall somewhat settles. These effects are due to the increased crossflow at this position, which becomes strong enough to deflect the wall jets formed from impingement, which can still sufficiently occur because of the small channel height. There seems to be a direct interaction between the sidewall HTC and the target surface profile, as they almost lie on top of each other in the upstream part of the channel. When comparing to the available impingement channel correlations, acceptable results are obtained at the first jet as well as from $X/D = 30$–70. The correlation seems to underpredict the values in the upstream section and then overpredict them in the downstream region. These discrepancies may be the result of the sidewall influence, which was not present in the experiments conducted by [2]. In the upstream region, the sidewalls tend to increase the heat transfer, because of the second impingement region that is developed from the wall jets impacting the side surfaces. However, as the crossflow develops significantly, the contribution of the sidewall is less, and the correlation tends to overpredict the recorded results, still within the uncertainty bands. The correlation tends to digress in regions for which the sidewall influence is large. It is also interesting to note how the smooth channel prediction comes close to the values predicted in [2], as well as those recorded beyond an X/D of 50. At this point, impingement effects are becoming minimal when compared with the crossflow effects. Nevertheless, the augmentation due to impingement produces some enhancement.

Similarly, case 2A averaged results are presented in Fig. 13. From this plot, it is evident that with the larger impingement height ($Z/D = 3$), the sidewall HTC values do not compare as well to the target surface. With the increased channel height, as was evident from the local HTC distributions, there is less influence from the target surface on the sidewall. The larger channel height creates lower crossflow velocities, which do not maintain the higher sidewall HTC values observed in the previous case. The sidewall profile tends to be more flat, with less evidence of impingement. Target HTC values fall within the uncertainty band of the existing correlation along the entire channel, again suggesting less influence from the sidewall. However, beyond the first three holes, the correlation tends to slightly underpredict the actual HTC values. The slight increase in turbulence due to the presence of the sidewall, although the coupling is weak, may be blamed for this inconsistency. Again, smooth pipe predictions approach the recorded values in the downstream regions. For this case, however, the enhancement due to impingement is larger, creating some augmentation even at the channel exit. Note, however, that for all cases, the impingement channel correlation approaches that of a smooth pipe when significant crossflow is present. The fact that the heat transfer becomes dominated by crossflow effects in the downstream regions is then more apparent.

Case 2B, shown in Fig. 14, yielded similar results to case 2A when considering the coupling between the sidewall and target surface. Again, the sidewall underperforms the target surface, as the effects of impingement are less apparent on this surface. As mentioned earlier, this case yielded the most uniform HTC values throughout the channel, suggesting an optimum configuration. However, the existing correlation does not yield very acceptable results for this configuration in the upstream regions. It significantly overpredicts the first few jets at or beyond the limits of the uncertainty band. Not until significant crossflow has developed does the correlation yield accurate results. However, after three jets, the results do overlap. The sidewalls may cause some recirculation that negatively affects the impingement at this location, causing lower HTCs in this region. Visualization methods are required to determine the exact phenomena that cause this discrepancy. Compared with the previous

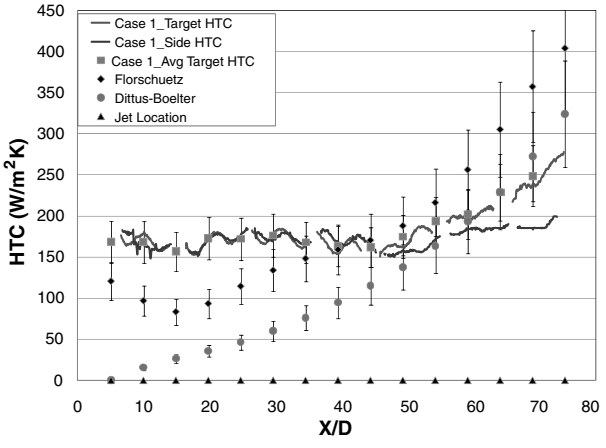

Fig. 12 Case 1 averaged heat transfer distribution.

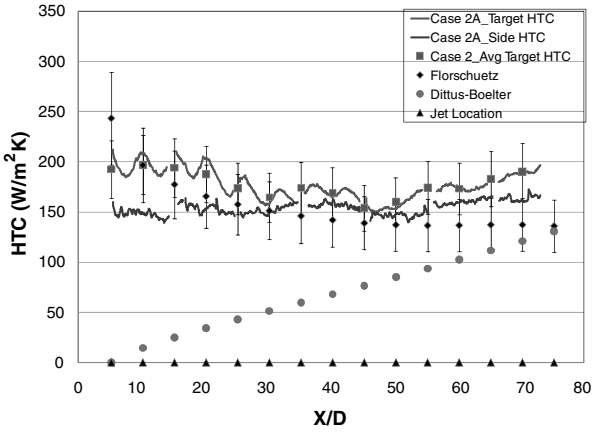

Fig. 13 Case 2A averaged heat transfer distribution.

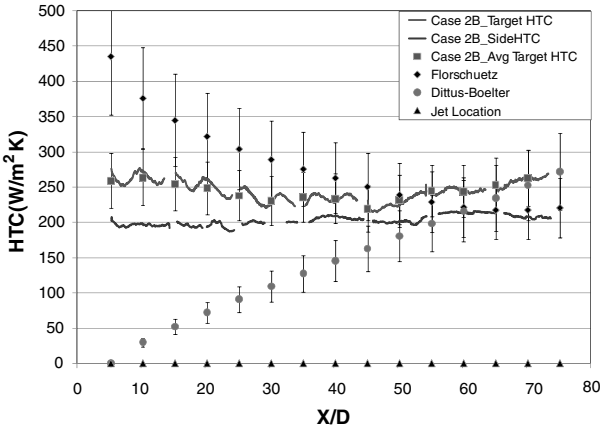

Fig. 14 Case 2B averaged heat transfer distribution.

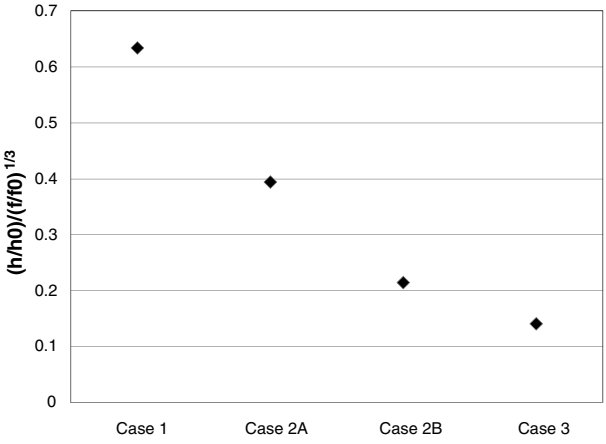

Fig. 16 Thermal effectiveness comparison.

case, there is less enhancement over smooth channel predictions in the downstream regions. Both the side and target walls approach the smooth channel predictions, whereas with case 2A, the target surface outperforms the sidewall and the smooth channel predictions near the channels exit. This increase in the Reynolds number also results in increased levels of turbulence. Therefore, any increased turbulence due to the presence of the downstream jets and sidewalls has less of an effect at high Reynolds numbers. At low Reynolds numbers, the incoming jets may act to increase the turbulence of the flow, even if no impingement successfully occurs.

Finally, at the largest impingement height, the two surfaces again seem to be only weakly coupled, as seen in Fig. 15. The target surface in this case outperforms the sidewall throughout the channel, due to the low crossflow velocities resulting from the large channel height. Again, there is no evidence of impingement along the sidewall, due to the large sidewall surface area, compared with the possible size of the wall jets (typically on the order of 1–2 jet diameters [14]). This case, however, matched the predicted results with surprising accuracy. It is also interesting to note that this case is beyond the parameters tested in the literature [2], for which maximum impingement heights of 3 diameters were tested. Nevertheless, the results match nicely. Throughout the channel, the correlation held well within the uncertainty bands of both sets of data. This agreement implies that, as the channel height is increased significantly, the sidewall coupling becomes less apparent, and traditional impingement channel correlations apply. However, with these cases, there is the drawback of lower HTCs along these sidewalls.

D. Thermal Effectiveness

To obtain a fair comparison of the performance of each channel configuration, the thermal effectiveness of each was compared. It is expected that there is a single case for which the increase in heat transfer outweighs the increase in pressure drop required. From the previous analysis, it was apparent that the enhancement of each configuration varies. Examining Fig. 16, we see that the effectiveness decreases as the channel height and Reynolds number increases. Although case 2B yielded the most uniform results, case 1 was most efficient when considering the pumping power required for each case. The high effectiveness values for case 1 can be attributed to the large heat transfer levels on the sidewalls, which were comparable with that on the target wall. Because of the small channel height, both the side and target surfaces benefited from the impingement features found within the channel. As the channel height increased, the heat transfer on the sidewalls was not as beneficial and lowered the channel average. Also, comparing cases 2A and 2B, as the Reynolds number increased, the effect of the jets was less significant when compared with traditional channel flow. It then becomes obvious that the best channel design, when considering the thermal effectiveness, would be that of a small channel height and lower Reynolds numbers. However, designers may have to consider other factors when designing impingement channels, such as profile uniformity.

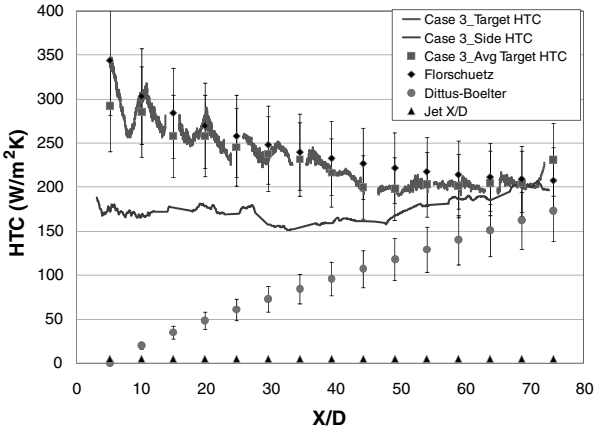

Fig. 15 Case 3 averaged heat transfer distribution.

V. Conclusions

It has been seen from this analysis that the sidewalls provide significant heat transfer from an impingement channel, especially with the development of a high-velocity crossflow. Sidewalls in channels with shorter impingement heights tend to perform better at a given average jet Reynolds number, due to the increased crossflow velocities and strong impingement effects on both the target and sidewall surfaces. However, this increase is at the penalty of larger channel pressure drops. It was also seen that, given a long enough channel, target walls also benefit from crossflow accumulation, especially at smaller Z/Ds. Case 2B yielded the most uniform sidewall results and provided the largest target surface results, whereas case 1 yielded the highest thermal effectiveness. According to these results, the increase in pressure drop required to push the flow through this small channel was outweighed by the increase in the heat transfer rates obtained. Because all efficiencies were below unity, the increase in heat transfer always yields a significant pressure drop. However, the absolute value of the effectiveness was highly dependent on the overall length of the channel. Heat transfer enhancement levels were very high at the start of the channel and decayed as the crossflow velocities increased. The pressure drop required to push the flow through the long channel is also significantly higher than that required for a channel with only a few jets. However, the same overall trend would be expected. This cooling technique proves to be an effective one, especially in situations that require large amounts of heat removal with low levels of coolant usage.

Although most of the existing literature has investigated multiple rows of jets, the fact that the sidewalls provide appreciable heat transfer suggests the opportunity for efficiently designed single-row impingement channels. It may be possible to extract additional heat

with the properly designed sidewalls. Care must be taken when applying correlations intended for large spanwise arrays to circumstances for which the sidewall influence is important.

It is evident that impingement channel cooling is an extremely effective method of heat removal with minimal coolant usage. The jets tend to not only augment heat transfer though impingement but also through the mixing and cooling of the crossflow.

Acknowledgment

Authors acknowledge the support of the State University System of the Florida Turbine Initiative, made possible by NASA Award NNC06GA17G.

References

[1] Taylor, J. R., "Heat Transfer Phenomena in Gas Turbines," ASME Turbo Expo, ASME Paper 80-GT-172, 1980.

[2] Florschuetz, L. W., Truman, C. R., and Metzger, D. E., "Streamwise Flow and Heat Transfer Distributions for Jet Array Impingement with Crossflow," *Journal of Heat Transfer*, Vol. 103, No. 8, 1981, p. 337.

[3] Florschuetz, L. W., and Isoda, Y., "Flow Distributions and Discharge Coefficient for Jet Array Impingement with Initial Crossflow," *Journal of Engineering for Power*, Vol. 105, April 1983, p. 296. doi:10.1115/1.3227415

[4] Florschuetz, L. W., Berry, R. A., and Metzger, D. E., "Periodic Streamwise Variations of Heat Transfer Coefficients for Inline and Staggered Arrays of Circular Jets with Crossflow of Spent Air," *Journal of Heat Transfer*, Vol. 102, Feb. 1980, pp. 132–137.

[5] Al-Aqal, O. M. A., "Heat Transfer Distributions on the Walls of a Narrow Channel with Jet Impingement and Crossflow," Ph.D. Dissertation, Mechanical Engineering Dept., Univ. of Pittsburgh, Pittsburgh, PA, 2003.

[6] Lucas, M. G., Ireland, P. T., and Wang, Z., "Fundamental Studies of Impingement Cooling Thermal Boundary Conditions," AGARD 80th PEP Symposium, AGARD Paper 14, 1992.

[7] Van Treuren, K. W., Wang, Z., and Ireland, P. T., "Detailed Measurements of Local Heat Transfer Coefficient and Adiabatic Wall Temperature Beneath an Array of Impinging Jets," *Journal of Turbomachinery*, Vol. 116, No. 3, 1994, pp. 369–374. doi:10.1115/1.2929423

[8] Son, C., Gillespie, D., Ireland, P., and Dailey, G., "Heat Transfer and Flow Characteristics of an Engine Representative Impingement Cooling System," *Journal of Turbomachinery*, Vol. 123, No. 1, 2001, pp 154–160. doi:10.1115/1.1328087

[9] Annerfeld, M., Johan, P., and Torisson, T., "Experimental Investigation of Impingement Cooling with Turbulators or Surface Enlarging Elements," ASME Turbo Expo, ASME Paper GT-0149, 2001.

[10] Mushatat, K. S., "Analysis of the Turbulent Flow and Heat Transfer of the Impingement Cooling in a Channel with Crossflow," *Journal of King Abdulaziz University: Engineering Science*, Vol. 18, No 2, 2007, pp 101–122.

[11] Liu, Q., and Kapat, J., "Study of Heat Transfer Characteristics of Impinging Air Jet Using Pressure and Temperature Sensitive Luminescent Paint," Ph.D. Dissertation, Mechanical Materials and Aerospace Engineering Dept., Univ. of Central Florida, Orlando, FL, 2006.

[12] Ricklick, M., Kersten, S., and Kapat, J. S., "Effects of Channel Height and Bulk Temperature Considerations on Heat Transfer Coefficient of Wetted Surfaces in a Single Inline Row Impingement Channel," 2008 ASME Heat Transfer Conference, ASME Paper HT2008-56323, 2008.

[13] Incropera, F. P., and DeWitt, D. P., *Fundamentals of Heat and Mass Transfer*, Wiley, Hoboken, NJ, 2002, pp. 491–493.

[14] Martin, H., "Impinging Jet Flow Heat and Mass Transfer," *Advances in Heat Transfer*, Vol. 13, 1977, pp. 1–60. doi:10.1016/S0065-2717(08)70221-1